Parallel variable-density spiral imaging using nonlocal total variation reconstruction*

Fang Sheng(方 晟)[a] and Guo Hua(郭 华)[b]†

[a] Institute of Nulcear and New Energy Technology, Tsinghua University, Beijing 100084, China
[b] Center for Biomedical Imaging Research, Department of Biomedical Engineering, School of Medicine, Tsinghua University, Beijing 100084, China

(Received 25 November 2013; revised manuscript received 19 December 2013; published online 18 March 2014)

The relatively long scan time is still a bottleneck for both clinical applications and research of magnetic resonance imaging. To reduce the data acquisition time, we propose a novel fast magnetic resonance imaging method based on parallel variable-density spiral acquisition, which combines undersampling optimization and nonlocal total variation reconstruction. The undersampling optimization promotes the incoherence of resultant aliasing artifact via the "worst-case" residual error metric, and thus accelerates the data acquisition. Moreover, nonlocal total variation reconstruction is utilized to remove such an incoherent aliasing artifact and so improve image quality. The feasibility of the proposed method is demonstrated by both numerical phantom simulation and *in vivo* experiment. The experimental results show that the proposed method can achieve high acceleration factor and effectively remove an aliasing artifact from data undersampling with well-preserved image details. The image quality is better than that achieved with the total variation method.

Keywords: magnetic resonance imaging, variable-density spiral, parallel imaging, nonlocal total variation

PACS: 74.25.nj, 61.05.Tv, 42.30.Wb **DOI:** 10.1088/1674-1056/23/5/057401

1. Introduction

Parallel imaging is one of the most effective ways to reduce the scan time of magnetic resonance imaging (MRI). It adopts multiple receiver coils to simultaneously acquire signals with a sub-Nyquist sampling rate. Such undersampled signals can be reconstructed into an un-aliased image via proper reconstruction algorithms,[1–7] provided that the sensitivity distribution of the receiver coils can be obtained. The most widely-used algorithms include sensitivity encoding (SENSE)[1] and generalized autocalibrating partially parallel acquisitions (GRAPPA).[5]

Among all of the parallel imaging reconstruction methods, SENSE provides a rigorous framework for parallel imaging with different k-space sampling trajectories.[8] However, like all parallel imaging methods, at high acceleration factors SENSE reconstruction can be ill-posed, which can lead to noise amplification in reconstructed images.[9] This becomes more severe as the acceleration factor increases.

One way to mitigate this problem is to use a non-uniform or random sampling sequence that has more uniform noise distribution. Variable density spiral (VDS)[10,11] is one such sequence, which oversamples central k-space data while maintaining fast k-space traversal speed. Due to such non-uniform sampling, the undersampling artifact of VDS appears to be incoherent (noise-like), and its intensity can be significantly lower than that from uniform undersampling.[10] Therefore, VDS has been used to accelerate the data acquisition for different applications, such as MR fluoroscopy,[12] cardiac imaging,[10] perfusion imaging,[13] and coronary MR angiography.[14] Recent compressed sensing (CS) theory further reveals that such aliasing artifacts can be removed via proper nonlinear reconstruction algorithms.[15,16]

Another way to solve the ill-posedness of parallel imaging reconstruction is regularization, which reduces noise level by incorporating prior information into the reconstruction. Various regularization techniques have been proposed for SENSE reconstruction.[17–19] One widely used technique is the total variation (TV) regularization which can suppress noise while preserving sharp edges.[20,21] However, a TV regularized image may suffer from staircase artifacts and texture loss due to its piecewise smooth assumption.

Recently, nonlocal total variation (NLTV),[22] which combines nonlocal mean[23] and TV, has been proposed to solve the texture loss problem of TV. However, there are very few reports about its usage for parallel imaging,[24] which is restricted to the Cartesian parallel imaging and needs the assistance of additional noisy SENSE reconstruction for nonlocal weight computation. This scheme may be inefficient when the SENSE reconstruction image is poor.

To achieve both high acceleration factor and better-preserved fine image details, a fast parallel imaging method based on VDS and nonlocal total variation regularization is proposed in this paper. The Bregman scheme is utilized to iteratively refine the regularized reconstruction for improved reconstruction accuracy. The feasibility of this method is

*Project supported by the National Natural Science Foundation of China (Grant Nos. 81101030 and 61271132).
†Corresponding author. E-mail: huaguo@tsinghua.edu.cn
© 2014 Chinese Physical Society and IOP Publishing Ltd

demonstrated by numerical phantom simulation and *in vivo* experiments. The results demonstrate that this method can effectively suppress noises in SENSE reconstruction while preserving image details. The image quality is better than the conventional TV method.

2. Model and method

2.1. Variable density spiral trajectory

VDS trajectory provides an efficient and flexible way to adjust k-space sampling density based on the requirement of various applications, in the form of[11]

$$k(\tau) = \lambda \tau^{\alpha} \mathrm{e}^{\mathrm{j}2\pi n\tau}, \tag{1}$$

where τ is a function of time and varies from 0 to 1, n is the turns of the spiral, λ is a constant determined by the imaging matrix size N and the field of view (FOV): $\lambda = N/(2\times \mathrm{FOV})$.

Since the trajectory starts with the slew rate limit and gradually changes to the gradient amplitude limit, the time function τ can be formulated using the following piecewise function:

$$\tau(t) = \begin{cases} \left[\sqrt{\dfrac{s_{\mathrm{m}}\gamma}{\lambda\omega^2}\left(\dfrac{\alpha}{2}+1\right)}\,t\right]^{1/(\alpha/2+1)}, \\ \quad 0 \le t \le \min(T_{\mathrm{s}2\alpha}, T_{\mathrm{es}}), \\ \left[\sqrt{\dfrac{\gamma g_{\mathrm{m}}}{\lambda\omega}(\alpha+1)}\,t\right]^{1/(\alpha+1)}, \\ \quad T_{\mathrm{s}2\alpha} \le t \le T_{\mathrm{ea}}, \end{cases} \tag{2}$$

where γ is the amplitude; $T_{\mathrm{s}2\alpha}$ is the transition time from the slew rate limited period to the amplitude limited period; T_{es} is the ending time of the slew rate limited period; T_{ea} is the ending time of whole trajectory; and α is a constant that controls the k-space sampling density along the radial direction. The minimum α is 1, which corresponds to a regular spiral. Increased α results in a VDS trajectory that samples more densely in the center of k-space. In order to reduce the aliasing artifact level, the sampling density parameter α is optimized by using the following worst-case residual error:

$$\varepsilon = \frac{1}{A}\int_0^{2\pi}\int_0^{k_{\max}} (1 - W \otimes C)^2 \,\mathrm{d}k\,\mathrm{d}\phi, \tag{3}$$

where W is the sampling density compensation function, C is the gridding kernel, $\otimes$ is the convolution operator, and A is the area of k-space coverage. Since W is the reciprocal of the sampling density, equation (3) is also a function of sampling density.

As mentioned in the previous literature,[25,26] the convolution of W and C equals a modulation transfer function that maps non-Cartesian data to Cartesian grids. In ideal cases, this function should be unity at all sampling coordinates. When undersampled, the aliasing artifact makes this modulation transfer function deviate from unity. By integrating this deviation over the entire k-space, Eq. (3) provides a total energy measurement of the aliasing artifact level. Figure 1 shows how the residual errors change with α for different reduction factors. When $R = 1$ and $R = 2$, the error curves almost overlap with each other, which indicates that increasing α does not change the residual errors much. As the reduction factors increase further, the residual aliasing deceases nearly exponentially with respect to increased α. Note that the residual errors remain relatively stable after α reaches three. Since a larger α will lead to a longer readout window, this may introduce more off-resonance induced blurring. Therefore, based on the worst-case energy, $\alpha = 3$ provides a reasonable trade-off between residual error and readout window.

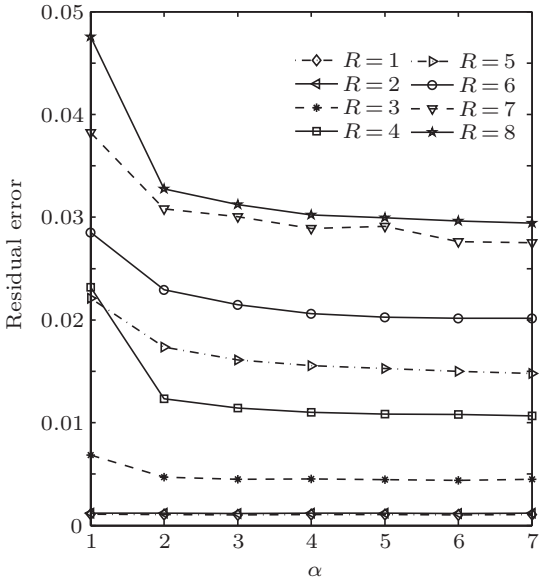


Fig. 1. The "worst-case" residual error of VDS with different sampling density parameter α for different reduction factors.

In practical implementation, the VDS trajectory of Eq. (1) is re-designed with a regularized slew rate function, so that the excessive magnitude of slew rate due to potential singularity of VDS at the k-space center can be avoided.

2.2. SENSE model

Parallel imaging uses phased array coils to simultaneously acquire a multi-channel MRI signal. For each coil, the acquired signal can be formulated as[8]

$$s_j(\boldsymbol{k}) = \int \rho(\boldsymbol{r}) C_j(\boldsymbol{r}) \mathrm{e}^{-\mathrm{i}\boldsymbol{k}\boldsymbol{r}} \,\mathrm{d}\boldsymbol{r}, \tag{4}$$

where $\rho(\boldsymbol{r})$ is the spin density spatial distribution of the scanned object, $C_j(\boldsymbol{r})$ is the sensitivity map of the j-th coil, $s_j(\boldsymbol{k})$ is the signal at k-space position $\boldsymbol{k}$ which is acquired by the j-th receiver coil. After discretization of Eq. (4), the following linear equation can be obtained:

$$\boldsymbol{d} = \boldsymbol{E}\boldsymbol{m}, \tag{5}$$

where $\boldsymbol{d}$ is a vector formed by k-space data derived from all the coils and $\boldsymbol{m}$ is an unknown vector formed by spin density of the scanned object. The system matrix $\boldsymbol{E}$ consists of the product of Fourier coefficient $e^{-i\boldsymbol{kr}}$ and the coil sensitivity $C_j(\boldsymbol{r})$.

Provided that the coil sensitivity can be obtained in advance, the desired image $\boldsymbol{m}$ can be reconstructed by inverting the system matrix $\boldsymbol{E}$ in Eq. (5). Since the direct inversion of system matrix $\boldsymbol{E}$ can be prohibitively difficult due to its huge size, equation (5) is usually solved using the following least square estimation:

$$\boldsymbol{m} = \arg\min \|\boldsymbol{E}\boldsymbol{m} - \boldsymbol{d}\|_2^2. \tag{6}$$

For Cartesian sampling trajectory, Eq. (5) can be decomposed into a series of small linear equations. However, for a non-Cartesian sampling trajectory such as VDS, this decomposition is not applicable. Thus, equation (5) is usually solved via some iterative linear numerical schemes, such as conjugate gradient algorithm[8] with non-uniform Fourier transform (NUFFT) or gridding method.

2.2.1. Regularized SENSE reconstruction

At high acceleration factors, the system matrix $\boldsymbol{E}$ can be ill-conditioned. Consequently, the least square estimation in Eq. (6) can lead to significant noise amplification. One effective method to stabilize Eq. (6) is to use regularization technique, which can be formulated as

$$\boldsymbol{m}^{\mu} = \arg\min_{\boldsymbol{m}}\{\|\boldsymbol{E}\boldsymbol{m} - \boldsymbol{d}\|_2^2 + \mu J(\boldsymbol{m})\}, \tag{7}$$

where $J(\boldsymbol{m})$ is the regularization term that adds prior knowledge about the imaging object into the reconstruction, and μ is the regularization parameter. The first term of Eq. (7) is the fidelity term that represents the bias from SENSE model. The second term is the regularization term that represents the bias from the prior knowledge. By tuning the regularization parameter μ, a tradeoff can be made between these two biases. To reduce noise level, a smoothing prior is usually used in Eq. (7), such as the popular TV method. The regularization term $J(\boldsymbol{m})$ of TV takes the form of $\|\nabla\boldsymbol{m}\|_1$, where ∇ is the discrete image gradient operator and $\|\cdot\|_1$ is the L1 norm that sums up the absolute value of elements in a vector. TV has been found to be effective in both suppressing noise and preserving sharp edges in various applications. The CS theory further demonstrates that TV promotes the sparsity of images in a finite difference domain and can effectively remove a noise-like aliasing artifact.

Since the aliasing artifacts of VDS appears incoherent, TV can be utilized to remove such pseudo-incoherent aliasing artifacts and enable further acceleration. However, TV may blur out low-contrast image structures and cause structure loss when imaging data are highly undersampled, which inevitably degrades the diagnostic information in images.

2.2.2. Nonlocal total variation regularization

NLTV improves fine structure preservation by extending the 4-neighborhood gradient in TV method to the following generalized discrete image gradient:[22]

$$\nabla_i^w \boldsymbol{m} = \sqrt{w(i,j)}[m(j) - m(i)], \quad i \in \Omega, \tag{8}$$

where m is the discrete image, and j is a pixel within the neighborhood of i. The neighborhood is defined as a square window that is centered at pixel i. For each pixel in an image, a neighborhood window is defined for computing the generalized derivative in Eq. (8). The weight $w(i,j)$ depends on the patch similarity between pixel i and j, which is defined as[23]

$$w_{ij}(i,j) = \frac{1}{W_i}\exp\left(-\frac{\|p(i) - p(j)\|_2^2}{\sigma^2}\right), \tag{9}$$

where $p(i)$ and $p(j)$ are image patches centered at pixel i and j, respectively; σ is the threshold parameter, which is usually determined by the background noise variance; and, W_i is the normalization factor that is a sum of all computed weights for the pixel i

$$W_i = \sum w_{ij}(i,j). \tag{10}$$

With the generalized image gradient in Eq. (8), the NLTV regularized SENSE reconstruction can be formulated as

$$\boldsymbol{m}^{\mu} = \arg\min_{\boldsymbol{m}}\left\{\|\boldsymbol{E}\boldsymbol{m} - \boldsymbol{d}\|_2^2 + \mu\|\nabla_i^w\boldsymbol{m}\|_1\right\}. \tag{11}$$

Equation (11) shows that NLTV shares the L1 norm with TV, which maintains the sparsity promotion property of TV. However, the generalized gradient used in NLTV involves more pixels into the constraint. Furthermore, intensities of these pixels are not uniformly penalized. The weights in Eq. (9) reveal the similarity between pixels in the N-neighborhood. Based on these weights, the L1-norm constraint is imposed allotropically to each pixel, which helps to avoid the over smoothing of pixels in fine image structures.

2.3. Bregmanized nonlocal total variation

The Bregman iteration scheme has been used in L1-norm related optimization, such as TV for alleviating the texture loss problem.[30] In order to further improve the reconstruction accuracy, this iterative scheme was applied to NLTV in this study. With NLTV, the Bregman iteration can be formulated as

$$\boldsymbol{m}_k^{\mu} = \arg\min_{\boldsymbol{m}}\{\|\boldsymbol{E}\boldsymbol{m} - \boldsymbol{d}\|_2^2 + \mu D_{\mathrm{NLTV}}(\boldsymbol{m}_{k-1}, \boldsymbol{m}_k)\}, \tag{12}$$

where $\boldsymbol{m}_k$ is the result of the k-th iteration, $D_{\mathrm{NLTV}}(\boldsymbol{m}_k, \boldsymbol{m}_{k-1})$ is the Bregman distance of NLTV function between the result of the k-th iteration and that of $(k-1)$-th iteration, which is defined as

$$D(\boldsymbol{m}_{k-1}, \boldsymbol{m}_k)$$

$$= \|\nabla_i^w \boldsymbol{m}_k\|_1 - \|\nabla_i^w \boldsymbol{m}_{k-1}\|_1 - \langle \nabla_i^w (\|\nabla_i^w \boldsymbol{m}_{k-1}\|_1), \boldsymbol{m}_k - \boldsymbol{m}_{k-1}\rangle, \quad (13)$$

where $\nabla_i^w \left(\|\nabla_i^w \boldsymbol{m}_{k-1}\|_1\right)$ is the gradient of NLTV function at $\boldsymbol{m}_{k-1}$. Equation (13) demonstrates that the Bregman distance is a measurement of the distance between increment of NLTV function from $\boldsymbol{m}_{k-1}$ to $\boldsymbol{m}_k$ and the corresponding tangent line increment. As pointed out by previous studies,[27] the Bregman iteration for a linear system can be equivalently formulated as

$$\boldsymbol{m}_k^{\mu} = \arg\min_{\boldsymbol{m}} \{\|E\boldsymbol{m} - (\boldsymbol{d} + \boldsymbol{u}_{k-1})\|_2^2 + \mu \|\nabla_i^w \boldsymbol{m}\|_1\}, \quad (14)$$

where $\boldsymbol{u}_k = \boldsymbol{u}_{k-1} + \boldsymbol{d} - E\boldsymbol{m}_k$. The intermediate variable $\boldsymbol{u}_k$ is a sum of results from previous iteration and components removed in historic iterations. This can be seen as "adding error back", which compensates the removed image structure in a previous iteration and improves the reconstruction accuracy. Another advantage introduced by the Bregman scheme is that its reconstruction result is insensitive to parameter selection, which increase the robustness of NLTV in the presence of imperfect parameter selection.

3. Experiment and results

3.1. Numerical simulation

The feasibility of the proposed method was first tested by numerical simulation using Shepp–Logan phantom. The images acquired by each coil were simulated by multiplying the Shepp–Logan phantom with a set of pre-acquired 8-channel coil sensitivity maps. A VDS trajectory that contains 24 interleaves was used in simulation, which is the same trajectory as that used in *in vivo* experiments. The VDS sampled k-space data of each coil were obtained by a non-uniform Fourier transform[28] of each coil image, respectively. To test the robustness of the proposed regularization algorithm, a spatially uniform and uncorrelated Gaussian white noise was added to the simulated VDS data of each coil. A reduction factor of 6 was used by retrospectively undersampling the obtained VDS data.

3.2. *In vivo* experiment

Two 25-year-old healthy volunteers were recruited and they provided their informed written consent for *in vivo* studies. A set of T2 weighted brain data were acquired on a Philips 3T system (Philips Healthcare, Best, The Netherland) using a spin echo variable density spiral sequence with an 8-channel head coil. The sequence has a TR/TE of 500/20 ms, 220×220 mm FOV, a slice thickness of 5 mm, and a resolution of 0.86×0.86 mm^2. The spiral readout contains 24 arms and each arm has 4335 samples. For the *in vivo* experiment, only five of a total of 24 interleaves were retrospectively extracted and used for reconstruction, which results in a net reduction factor of 4.8.

3.3. Algorithm implementation

The undersampled VDS data were reconstructed by: 1) un-regularized SENSE, 2) TV regularization, and 3) the proposed NLTV. To be consistent in computation, all of the reconstruction methods in this study were implemented by the proximal forward–backward algorithm.[29] For all the three methods, the iteration was stopped when the decrease of object function between two iterations was smaller than 0.01%.

Since the Bregman iteration is used, the NLTV method becomes relatively insensitive to the selection of certain parameters. In this study, different search windows and patch sizes have been tested to optimize the NLTV. As expected, the reconstruction results do not show obvious differences for both qualitative and quantitative evaluations. Since an increased patch and search window size can significantly prolong the computation time, intermediate values for both sizes are preferred. Therefore, the patch and search window size of NLTV were fixed as 3×3 and 11×11, respectively, for all of the experiments. The threshold parameter in Eq. (9) was estimated based on the background noise variance, which has been proved to yield satisfied results in image filtering tasks.[23] For both TV and NLTV, the regularization parameter was selected from a geometric range based on the root mean square error (RMSE) with respect to the reconstruction results of fully sampled data. The off-resonance was corrected using an improved automatic off-resonance correction.[31]

3.4. Results and discussion

Figure 2 shows the k-space trajectory of a single-arm from the VDS pulse sequence optimized based on Eq. (3). This trajectory samples the center of k-space with a rate higher than Nyquist rate. As the radius of spiral increases, the sampling rate is gradually reduced (see Fig. 2(a)). As presented in Fig. 2(b), the sampling rate of VDS exponentially changes from oversampling to undersampling. A total of 164 data points are sampled at a rate no less than the Nyquist rate, while the other 4171 data points are sampled at a rate less than Nquist rate in this special case.

The convergence behavior of the NLTV reconstruction is demonstrated with the *in vivo* experiment data for a reduction factor of 4.8 in Fig. 3. The RMSE drops quickly in the first seven iterations, and reaches its minimum at about the fifth iteration. This convergence behavior is very typical for non-Cartesian trajectory reconstruction.[32]

Figure 4 compares the numerical simulation results for a reduction factor of 6. The SENSE image shows significantly amplified noise, which implies that, with given coil sensitivity, the SENSE reconstruction at such high acceleration is quite ill-posed. Such noise not only degrades the signal-to-noise ratio (SNR), but also deteriorates local image structures. Although

TV effectively suppresses the amplified noise, the local structures and edges are considerably blurred. In addition, there is an artificial intensity variation across the whole image. In comparison, the NLTV image shows much sharper edges and well-preserved, fine image details. The difference maps at the bottom of Fig. 4 reveal that TV has a high level of structural error at edges and details together with contrast loss. In comparison, the NLTV is visually free of the contrast loss problem and shows a much lower level of structural error.

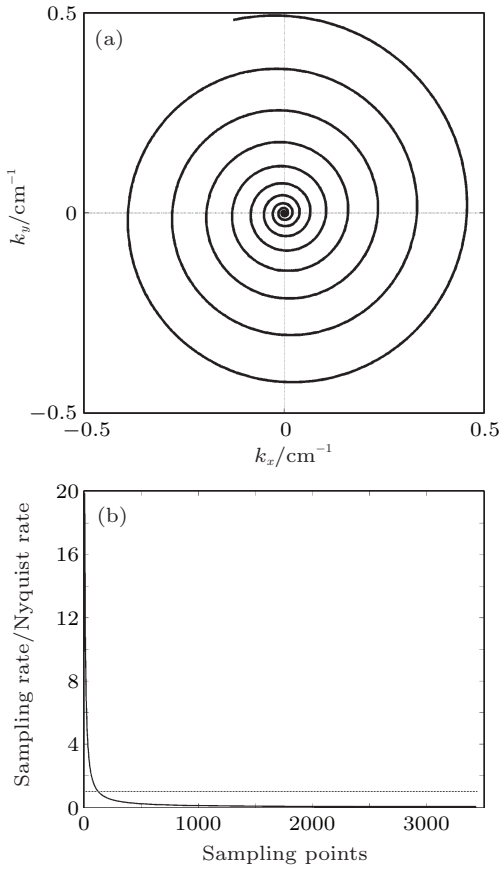


Fig. 2. The *k*-space trajectory of the optimized VDS pulse sequence. (a) The *k*-space trajectory of a single arm from VDS, (b) the sampling rate of a single arm from VDS. The dashed line in panel (b) indicates the Nyquist sampling rate.

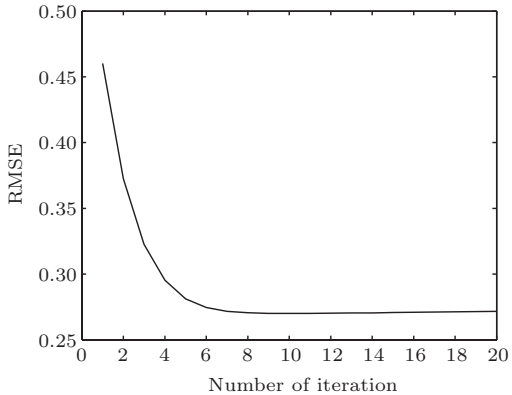


Fig. 3. Convergence behavior of the NLTV for *in vivo* VDS experiment with a reduction factor of 4.8.

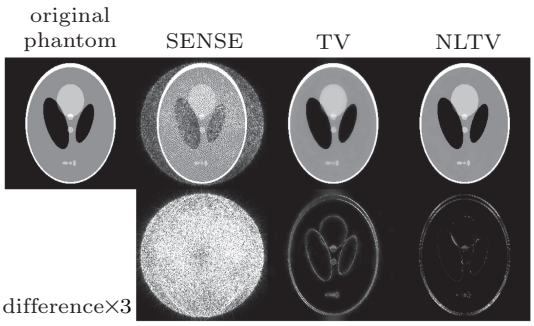


Fig. 4. Numerical phantom simulation results for a reduction factor of 6. The top row shows the reference image and the SENSE image. The columns, from left to right, are reference image and results of SENSE, TV, and NLTV for the top panel. The bottom panel shows difference maps of SENSE, TV, and NLTV with respect to the reference image, respectively (scaled by a factor of 3 for better visualization).

Image detail preservation of different reconstruction algorithms can be better visualized from the center vertical line plot from the reconstructed images in Fig. 5. The SENSE plot

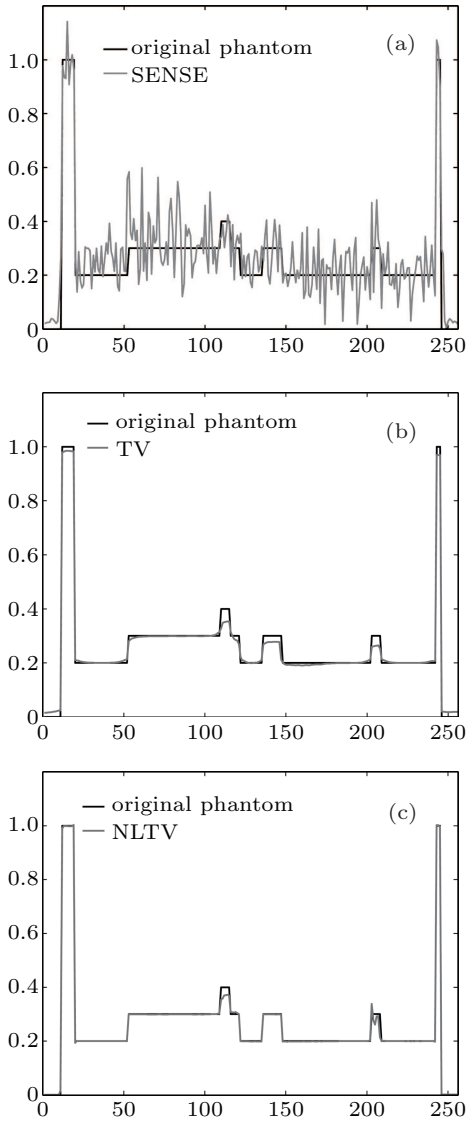


Fig. 5. Cross section plots of images reconstructed by different methods for a reduction factor of 6: (a) SENSE; (b) TV regularization; (c) NLTV.

exhibits a large oscillation (see Fig. 5(a)). TV effectively removes such oscillation, but suffers from contrast loss, which is demonstrated as the shrinkage of structure edges. Meanwhile, the shape of edges in the TV plot is blurred considerably. Such blurring also causes artificial intensity changes in a flat area (see Fig. 5(b)). In contrast, although there is also some edge shrinkage for small image structures, the NLTV plot matches the original phantom plot exactly for most parts of the plot.

Figure 6 compares *in vivo* VDS images reconstructed by SENSE, TV, and NLTV. Similar to the numerical simulation, the SENSE image shows amplified noise. However, the noise distribution of VDS is much more uniform than that of traditional Cartesian undersampling,[19] which yields a better visual effect. Although TV effectively removes noise, it also blurs the image. Some fine image structures are lost due to this blurring effect (indicated by the arrow in Fig. 6), which comprises the overall image quality. In contrast, the proposed NLTV method not only removes the severe noise in the SENSE image, but also maintains sharper structures than the TV method. The second row of Fig. 6 shows the corresponding difference maps of each reconstruction method. For the SENSE, the reconstruction error behaves as amplified noise in the difference map. TV shows a high level of structural error both near the skulls and the ventricles. For NLTV, the total error level is the minimum of all three compared methods. Specifically, the structural error level is also much lower than that of TV.

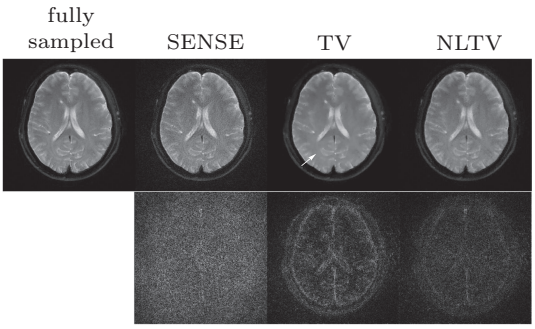


Fig. 6. *In vivo* experiment results for a reduction factor of 4.8. The top row shows the reference image and the SENSE image. The columns, from left to right, are reference image and results of SENSE, TV, and NLTV for the top panel. The bottom panel shows difference maps of SENSE, TV, and NLTV with respect to the reference image, respectively.

The fine-structure preservation performance of different methods for *in vivo* experiments can be better visualized with the zoomed-in images in Fig. 7. Both the noise in the SENSE image and the blurring effect in TV image degrades low-contrast structure. Meanwhile, TV also shows unacceptable stair-casing artifact. In comparison, the fine structure in the NLTV image is much better preserved and matches the fully sampled image well.

Table 1 summarizes the root mean square error (RMSE) of reconstructed images in all experiments. SENSE shows the largest RMSE, due to severely amplified noise. Compared with SENSE, both TV and NLTV effectively reduce the RMSE of the reconstruction. However, NLTV is more effective in the sense that its RMSE is the smallest among all of the test reconstruction methods.

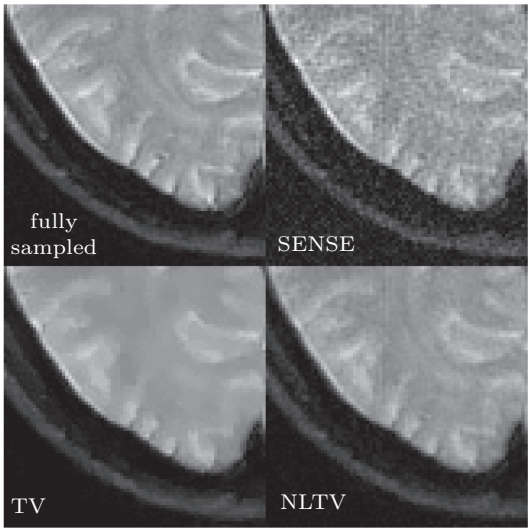


Fig. 7. Zoomed-in part of the *in vivo* experiment results for a reduction factor of 4.8.

Table 1. RMSE of image reconstructed by SENSE, TV, and NLTV.

Data set	SENSE	TV	NLTV
Numerical simulation	0.125	0.013	0.009
in vivo experiment	0.343	0.234	0.167

4. Conclusion

A fast parallel variable density imaging method has been proposed based on optimized VDS acquisition and NLTV reconstruction. This method minimizes the aliasing artifact energy through the "worst-case" residual error metric for VDS sequence design, so that the incoherence of the aliasing artifact can be promoted. The NLTV reconstruction suppresses such incoherent aliasing and amplified noise due to the ill-posedness of reconstruction. The experimental results demonstrate that this method can more effectively suppress noise amplification and preserve finer image details than the traditional TV method, which has high reduction factors.

References

[1] Pruessmann K P, Weiger M, Scheidegger M B and Boesiger P 1999 *Magn. Reson. Med.* **42** 952
[2] Griswold M A, Jakob P M, Nittka M, Goldfarb J W and Haase A 2000 *Magn. Reson. Med.* **44** 602
[3] Liu C, Bammer R and Moseley M E 2007 *Magn. Reson. Med. C* **58** 1171
[4] Sodickson D K and Manning W J 1997 *Magn. Reson. Med. C* **38** 591
[5] Griswold M A, Jakob P M, Heidemann R M, Nittka M, Jellus V, Wang J, Kiefer B and Haase A 2002 *Magn. Reson. Med.* **47** 1202
[6] Yeh E N, McKenzie C A, Ohliger M A, Sodickson D K and Foundation W 2005 *Magn. Reson. Med.* **53** 1383

[7] Kyriakos W E, Panych L P, Kacher D F, Westin C F, Bao S M, Mulkern R V and Jolesz F A 2000 *Magn. Reson. Med.* **44** 301
[8] Pruessmann K P, Weiger M, Bornert P and Boesiger P 2001 *Magn. Reson. Med.* **46** 638
[9] Lin F H, Kwong K K, Belliveau J W and Wald L L 2004 *Magn. Reson. Med.* **51** 559
[10] Tsai C M and Nishimura D G 2000 *Magn. Reson. Med.* **43** 452
[11] Kim D H, Adalsteinsson E and Spielman D M 2003 *Magn. Reson. Med.* **50** 214
[12] Spielman D M, Pauly J M and Meyer C H 1995 *Magn. Reson. Med.* **34** 388
[13] Lee J H, Hargreaves B A, Hu B S and Nishimura D G 2003 *Magn. Reson. Med.* **50** 1276
[14] Santos J M, Cunningham C H, Lustig M, Hargreaves B A, Hu B S, Nishimura D G and Pauly J M 2006 *Magn. Reson. Med.* **55** 371
[15] Donoho D L 2006 *IEEE Trans. Inf. Theory* **52** 1298
[16] Lustig M, Donoho D L and Pauly J M 2007 *Magn. Reson. Med.* **58** 1182
[17] Liu B, King K, Steckner M, Xie J, Sheng J and Ying L 2009 *Magn. Reson. Med.* **61** 145
[18] Ying L, Liu B, Steckner M C, Wu G, Wu M and Li S J 2008 *Magn. Reson. Med.* **60** 414
[19] Fang S, Ying K, Zhao L and Cheng J P 2010 *Magn. Reson. Med.* **64** 1413
[20] Rudin L, Osher S and Fatemi E 1992 *Magn. Reson. Med.* **60** 259
[21] Block K T, Uecker M and Frahm J 2007 *Magn. Reson. Med.* **57** 1086
[22] Zhang X Q, Burger M, Bresson X and Osher S 2010 *SIAM J. Imag. Sci.* **3** 253
[23] Buades A, Coll B and Morel J M 2006 *Multiscale Model. Simul.* **4** 490
[24] Liang D, Wang H, Chang Y and Ying L 2011 *Magn. Reson. Med.* **56** 1384
[25] Jackson J I, Meyer C H, Nishimura D G and Macovski A 1991 *IEEE Trans. Med. Imag.* **10** 473
[26] Winkelmann S, Schaeffter T, Koehler T, Eggers H and Doessel O 2007 *IEEE Trans. Med. Imag.* **26** 68
[27] Osher S, Burger M, Goldfarb D, Xu J and Yin W 2006 *Multiscale Model. Simul.* **4** 460
[28] Fessler J A and Sutton B P 2003 *IEEE Trans. Sig. Proc.* **51** 560
[29] Combettes P and Wajs V 2006 *Multiscale Model. Simul.* **4** 1168
[30] Fang S, Wu W C, Ying K and Guo H 2013 *Acta Phys. Sin.* **62** 048702 (in Chinese)
[31] Man L C, Pauly J M and Macovski A 1997 *Magn. Reson. Med.* **37** 906
[32] Qu P, Zhong K, Zhang B, Wang J and Shen G 2005 *Magn. Reson. Med.* **54** 1040